Pergamon

Canadian Metallurgical Quarterly, Vol. 34, No. 1, pp. 73–84, 1995

0008–4433/95 $9.50 + 0.00

0008–4433(94)00015–8

TECHNIQUE FOR THE ESTIMATION OF THERMAL RESISTANCE AT SOLID METAL INTERFACES FORMED DURING SOLIDIFICATION AND MELTING

NORMAN J. GOUDIE and STAVROS A. ARGYROPOULOS*

Department of Metallurgy and Materials Science, University of Toronto, 184 College St, Toronto, Ontario, M5S 1A4, Canada

(*Received* 14 *December* 1993; *in revised form* 22 *March* 1994)

Abstract—The early stages of melting and/or dissolution of additions to liquid metals or slags involve the formation and melting back of a shell composed of solidified liquid. This constitutes a moving boundary problem which is further complicated by evidence of an interface thermal resistance. It is during this period that a thermal resistance exists at the addition–shell interface. In this paper, a technique is presented for the estimation of this resistance. Data, collected from experiments, were used as input to a model which solves the inverse heat conduction problem in terms of a resistance estimate. Validation procedures were developed which authenticate both the collected data from experiments as well as the model results. Results for a variety of metal combinations have shown a relationship between the estimated thermal resistance and the expansion of the added metal. Specifically, the ratio between the added and solidified liquid metal expansion coefficients indicates the relative magnitude of the thermal resistance.

Résumé—Les premiers stades de fusion et/ou de dissolution d'additifs incorporés à des métaux en fusion ou à des scories, impliquent la formation et la re-fusion d'une croûte formée de liquide solidifié. Ceci constitue un problème de frontières mobiles, encore plus compliqué par l'évidence d'une résistance thermique d'interface. C'est pendant cette période que la résistance thermique se forme à l'interface additif–croûte. Cet article présente une technique permettant d'estimer cette résistance. Les données obtenues au cours des expériences furent utilisées comme données d'un modèle résolvant le problème de la conduction inverse de la chaleur, en terme d'une estimation de la résistance. On a développé des procédures de validation qui vérifient les données recueillies, tout comme les résultats du modèle. Les résultats pour différentes variétés de combinaisons de métaux ont montré l'existence d'une relation entre la résistance thermique estimée et l'expansion du métal ajouté. Plus précisément, le rapport entre les coefficients d'expansion des additifs et du métal solidifié indique la valeur relative de la résistance thermique.

NOMENCLATURE

α	thermal diffusivity, m^2/s
C_p	heat capacity of the addition, J/kgK
dr	distance between nodal points, m
Δr	distance of the shell thermocouple junction from the addition–shell interface, m
δr_N	effective radial distance from the last nodal point to the addition–shell interface, m
δr_{shell}	effective radial distance from the addition–shell interface to the shell thermocouple junction position, m
dt	numerical time step, s
ξ_n	positive roots of the transcendental equation
F_o	Fourier number
γ	linear thermal expansion coefficient, 1/K
h_c	convective heat transfer coefficient, W/m^2K
J_0	1st Bessel function of the first kind
J_1	2nd Bessel function of the first kind
k_a	thermal conductivity of the addition, W/mK
K_a	thermal coefficient embodying the conductivity of the addition and the thermal resistance at the interface, W/mK
k_s	thermal conductivity of the shell metal, W/mK
K_s	thermal coefficient embodying the conductivity of the shell metal and the thermal resistance at the interface, W/mK
L_s	latent heat of the shell metal, J/kg
n	nodal point
N	denotes the last node in the nodal network
q''	heat flux, W/m^2
RAD	radius of the cylindrical addition, m
r	radial distance, m
r_N	radial distance to the last nodal point, m
r_{shell}	radial distance to the shell thermocouple junction position, m
r^*	dimensionless radial distance
R_T	thermal resistance, m^2K/W
ρ	density of the addition, kg/m^3
S	shell thickness, m
T	temperature, K
$T(r, t)$	temperature in the addition as a function of r and t, K
$T_a(t)$	addition–side interface temperature, K
T_{bath}	temperature of the liquid bath, K
$T_c^m(t)$	measured centreline temperature, K
$T_c^c(t)$	calculated centreline temperature, K
T_{mp}	melting point temperature of the shell metal, K
$T_n(t)$	temperature of the nth node at an iterative time step, t, K
$T_n(t-1)$	temperature of the nth node at the previous iterative time step, t, K

* e-mail: argyro@ecf.utoronto.ca.

Table 1. Review of related thermal resistance investigations

Year	Author(s)	Experimental configuration			$R_T \times 10^5$ (m^2K/W)
		Design	Solid	Liquid	
1969	Levy *et al.* [3]	Investment cast around a locking chill (cylinder)	Aluminum	Aluminum alloy 7075	12
1970	Sun [4]	Cylinder immersion	Aluminum	Aluminum	22–88
			Copper	Aluminum	29–78
			Cast iron	Aluminum	23–78
1972	Prate and Biloni [5]	Bar-type, horizontal, axial cast	Al–5Cu alloy	Copper	9
			Aluminum	Copper	20
1977	Robertson and Fascetta [6]	Vertical, axial cast on flat chill	Copper	Tin	24
1977	Mucciardi [7]	Cylinder immersion	Aluminum	Lead	19
1978	Garcia and Prate [8]	Vertical, axial cast with water cooled, flat chill	1030 steel	Aluminum	20
1985	Ho and Pelke [9]	Vertical, axial cast with water cooled, flat chill	Copper	Aluminum	83
1991	El-Mahallawy and Assar [10]	Vertical, axial cast with water cooled, flat chill	Copper	Aluminum	8–50

$T_N(t)$ temperature of the last node prior to the interface, K
T_0 initial temperature of the addition, K
$T_s(t)$ shell–side interface temperature, K
$T^m_{shell}(t)$ measured shell temperature, K
θ^* dimensionless temperature
t time, s
t_{total} total time of calculations, s
V_n control volume for each node, m^3

INTRODUCTION

In a review of contact heat transfer research, Madhusudana and Fletcher [1] indicated a wide range of applications where heat flowing across an interface becomes important. Nuclear reactor applications, for example, require high thermal conductances whereas storage of cryogenic liquids require high thermal resistances. Information regarding the thermal characteristics of these interfaces is, therefore, critical. These are, however, examples relating to solid surfaces contacting in a mechanical fashion. Interfaces of metallurgical interest can become somewhat more complicated. For instance, a substantial heat flow barrier can be produced at the interface between a mould and solidifying metal during casting. Numerous papers [2–10] have been published dealing with this particular problem, which typically involves the formation of an air gap at the interface. Kumar and Prabhu [2] expressed the importance of interface heat transfer relating to the solidification of alloys in metallic moulds. Gravity/pressure die casting, continuous casting and squeeze casting were given as examples of processes where product quality can be affected by the interface thermal conditions. Table 1 chronologically outlines work similar to that investigated in this paper. Data reported by the referenced work have been tabulated in terms of thermal resistances for comparison purposes. Notably, most of the investigations used casting experiments, whereas Sun [4] and Mucciardi [7] used immersion methods.

Another area which can benefit is that of estimating other thermophysical properties and parameters such as those related to molten slags and fluxes. Once the thermal resistance at the interface is characterized, computational models can be extended to estimate both solid and liquid slag thermophysical data: effective thermal conductivities, for example. Casting fluxes is one application where such knowledge is beneficial. Here the continuous casting fluxes are used to enhance mould heat transfer, as well as to provide lubrication between the mould and solidifying steel. The result is a variety of heat transfer situations along the mould length. This variability necessitates knowledge of thermal resistance in the continuous casting mould.

In modelling the melting and/or dissolution of additions to liquid metals or slags, the early stages involve formation and melting back of a shell composed of solidified metal. Figure 1 illustrates schematically how the shell quickly forms then begins a slower melting back. This represents a moving boundary problem which is further complicated by evidence of a thermal resistance at the addition–shell interface. The heat transfer characteristics differ from those of the metal-mould in that no obvious air gap is formed. Instead, thermal expansion of the addition and contraction of the shell should increase the interfacial heat flow. In other words, a lowering of the thermal resistance is expected. Studying and estimating thermal resistances at these interfaces can help to understand the rate phenomena of alloy additions, as well as early solidification rates for thin castings.

This paper presents a technique for estimating such resistances. Experiments involving the immersion of solid metals into liquid metals were performed. In addition, a computer model was developed to perform the thermal resistance estimations. Validation procedures were developed which enable authentication of both the collected data from experiments as well as the model results. Current methods for estimating thermal resistances require complete knowledge of thermophysical properties of materials used. The present technique has an advantage over other methods because it is capable of estimating thermal resistances with little knowledge of the thermophysical properties of the solidifying metals.

Estimating parameters, such as thermal resistance, is generally performed by using an inverse technique. The inverse problem, in this work, is referred to as an inverse heat conduction problem (IHCP). A brief discussion of the theory and techniques of the IHCP follows. Interested readers can find further details on this subject in Refs [11–14].

Inverse heat conduction problem (IHCP)

Inverse techniques, in essence, estimate parameters or properties by extrapolating from defined conditions. Consider a steady

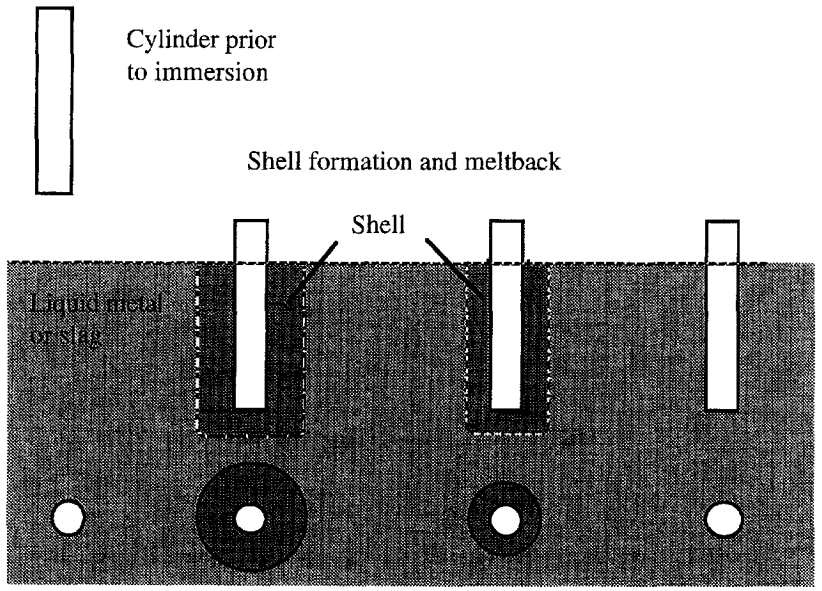

Fig. 1. Shell formation and melting back on a metal cylinder immersed into a liquid metal or slag.

state heat conduction situation as shown in Fig. 2(a). The direct problem involves solving for the temperature distribution within a domain knowing the boundary conditions; in this case, T_1 and T_2. An IHCP [Fig. 2(b)] involves estimating an unknown boundary condition which is difficult if not impossible to measure directly. Temperature measurements remote from the unknown boundary create a direct problem which is then used to estimate the unknown condition.

The technique is generally straightforward in steady state problems; however, it becomes more sensitive to measurement errors when highly dynamic systems are tackled. Features of the technique, shown in Fig. 3, include knowing a boundary condition, T_2, the geometry, L, and the sensor position, x'. It is generally assumed that these are known accurately; therefore, errors in estimating the unknown boundary condition arise mainly due to the sensor measurements. This is a key point in the IHCP; accurate and precise temperature data are a must.

The normal IHCP involves solving for a heat flux or temperature; however, other parameters, such as heat transfer coefficients, can also be estimated. These problems are referred to as inverse heat transfer coefficient problems (IHTCP). Interface resistances are effectively a subset of IHCP, and are solved in a similar fashion to the IHTCP. Curve fitting is a useful tool for estimating solutions to the IHCP. This technique allows a visualization of responses to the parameter being studied. In so doing, the investigator tries to best fit a calculated value to that known. Minimizing a least-squares fit of the error between the calculated and measured value for the property within the direct solution domain follows much the same principles. The advantage of the least-squares approach is that a mathematical criterion is set by which the best fit can be obtained. A further advantage of this approach is that time-dependent values for the condition can be estimated. For instance, a highly dynamic heat flux can be estimated sequentially by dividing the heat flux

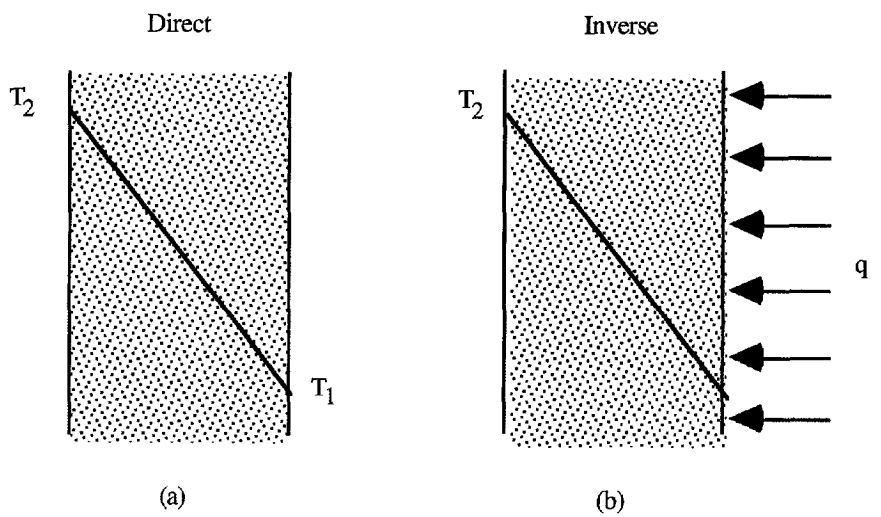

Fig. 2. Schematic example of (a) direct and (b) inverse heat conduction through a wall.

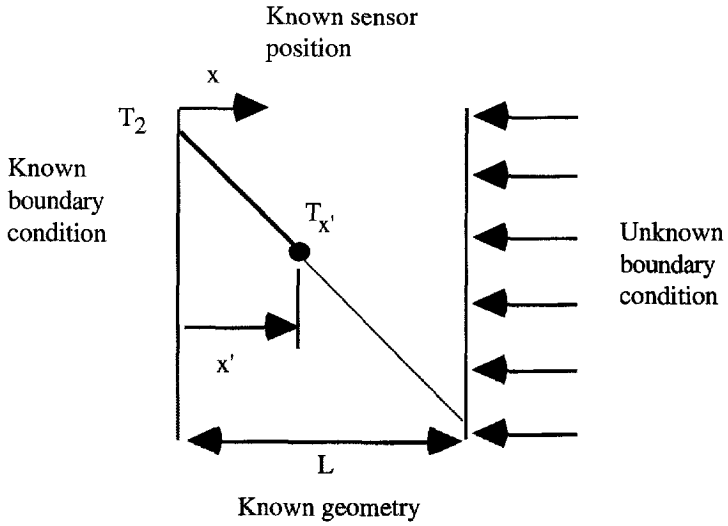

Fig. 3. Schematic illustration showing features of the inverse heat conduction problem (IHCP).

into components which can be calculated for different intervals over the time domain.

EXPERIMENTAL

In the present work an immersion technique involving the near-instantaneous immersion of cylindrical metal specimens into superheated liquid metal was utilized. Commercially pure aluminum (Al), copper (Cu), molybdenum (Mo) and titanium (Ti) rod stock, and cast Sorel iron (Fe) cylinders were used for the specimen metals. Bath metals included commercially pure (Al), lead (Pb) and tin (Sn). The specimen geometry was chosen such as to minimize heat flow end effects thereby creating a one-dimensional heat flow situation. A 10:1 length-to-radius was chosen as a reasonable approximation to the infinite cylinder [15].

Experiments were performed with three specimen configurations—Fig. 4: type A three-bore and types B and C centreline-bore. Each specimen was prepared by cutting and facing the rod, or cast cylinder, to a 15.2 cm (6″) length then turning to the 2.54 cm (1″) diameter. The Mo was received at the desired geometry. Holes—0.3 cm (1/8″) in diameter—were drilled in accordance with the configuration desired. Each was wiped free of excess oils and drillings, cleaned in soapy water to remove any remaining extraneous materials and then washed with ethanol. Finally, each specimen was ground with grit paper while turning in a lathe to provide a consistent surface finish. A final wash and ethanol wipe was performed before using the specimens.

Type-K thermocouples were constructed with 0.0127 cm (0.005″) diameter wire, and protected with 0.238 cm (3/32″) diameter, double bore alumina sheathes. The thermocouples were fixed as shown in Fig. 4 to facilitate temperature measurements within the cylinder and along the surface. Shell thermocouples were fixed rigidly such that thermocouple junctions were 0.025–0.1 cm from the interface. Specific distances from the interface were noted prior to immersion. A comparison of the shell formation was performed by withdrawing specimens from the bath at intervals of approximately 5, 10 and 15 s. Shells formed on the type B configured specimens were not complete where the alumina sheath was fixed, whereas shells formed on type C configured specimens were uniform and complete. The type C configuration became the standard since it also provided the closest positioning of the junction. All thermocouple assemblies had bare junctions enabling good surface contact and reducing any thermal lag. A 30° superheat (SPH) was used for the experiments although some lower SPHs were tested. Immersions lasted 100 s, providing ample time for shell formation, melt back, and heating of the cylinder to the bath temperature. Data were collected at 0.1 s intervals with an intelligent satellite microperipheral.

NUMERICAL MODEL

The heat energy equation, in cylindrical coordinates, was applied to the experimental configuration. A simplified transient model for estimating the interface thermal resistance was devised by assuming that 1-dimensional, radial heat flow dominates during the life of the shell. The unsteady, 1-dimensional, radial conduction equation with constant thermophysical properties can be written for the cylinder:

$$0 \leqslant r \leqslant RAD, \quad 0 \leqslant t \leqslant t_{\text{total}}$$

$$\frac{k}{r}\frac{\partial}{\partial r}\left(r\frac{\partial T(r,t)}{\partial r}\right) = \rho C_p \frac{\partial T(r,t)}{\partial t}. \tag{1}$$

Prior to immersion, the temperature of the cylinder can be taken to be uniform at T_0. This initial condition can be expressed as

$$\text{for } t = 0 \text{ and } 0 \leqslant r \leqslant RAD, \quad T = T_0. \tag{IN-1}$$

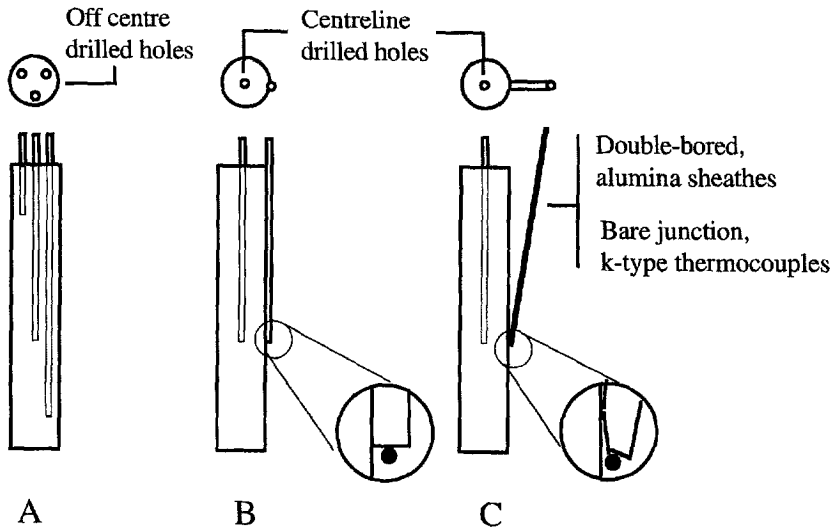

Fig. 4. Specimen configurations: three thermocouples (A); two thermocouples, one in the centreline (B) and another at the cylinder's edge (C).

Two boundary conditions apply during the heating of the cylinder. These can be expressed as

$$0 \leqslant t \leqslant t_{\text{total}} \text{ at } r = 0, \quad \frac{\partial T(0,t)}{\partial r} = 0 \qquad \text{(BC-1)}$$

and

$$0 \leqslant t \leqslant t_{\text{total}} \text{ at } r = RAD, \quad q'' = \frac{T_s(t) - T_a(t)}{R_T} \qquad \text{(BC-2)}$$

where R_T is the interface thermal resistance to the heat flux, q'', at the addition–shell interface located at radius RAD. The two temperatures, $T_a(t)$ and $T_s(t)$, describe the temperature drop at the interface as shown in Fig. 5. By assuming quasi-steady state conditions at the addition–shell interface, for any instant, a heat balance was performed which provided the following equations for the interface temperatures. The derivation of the equations is presented in Appendix A.

$$T_a(t) = R_T\left(\frac{R_T K_s k_a T_N(t) + \delta r_N k_s T^m_{\text{shell}}(t)}{R_T^2 K_a K_s - \delta r_N \delta r_{\text{shell}}}\right) \qquad (2)$$

$$T_s(t) = \frac{k_s R_T T^m_{\text{shell}}(t) + \delta r_{\text{shell}} T_a(t)}{R_T K_s} \qquad (3)$$

where

$$\delta r_N = RAD \ln\left(\frac{RAD}{RAD - \mathrm{d}r/2}\right)$$

$$\delta r_{\text{shell}} = RAD \ln\left(\frac{RAD + \Delta r}{RAD}\right)$$

$$K_a = k_a + \frac{\delta r_N}{R_T}$$

$$K_s = k_s + \frac{\delta r_{\text{shell}}}{R_T}.$$

A Fortran 77 code was written using the explicit form of the finite difference method. Briefly, a nodal network was established with the first node at the centre of the cylindrical domain and the last node at one-half the nodal spacing, dr, from the interface at RAD. This last node was designated as node N, and accounts for the dr/2 which occurs in the calculations involved in equations (2) and (3). The stability criteria for the radial case requires a Fourier number (Fo) <0.25 and was maintained below this value, thereby ensuring both stability and accuracy of solutions. Thermophysical and numerical data used in the computations are given in Tables 2 and 3, respectively. Temperature data collected from experiments were read from data files during the calculations. The shell temperature, T^m_{shell}, measured at 0.1 s intervals, was used in equations (2) and (3) to calculate the interface temperatures, $T_s(t)$ and $T_a(t)$, calculated at 0.0001 s intervals. The code then calculated the centreline temperature, $T^c_c(t)$, which was then used for curve fitting. Graphical curve fitting was used to initially define the range of thermal resistance values which applied to the given metal combinations.

The code was validated with two tests. Firstly, numerical results from the code were compared with the analytical solution for convective heat transfer to an infinite cylinder. Secondly, an integral heat balance was performed to estimate accuracy. Heat balance calculations showed that the heat content and interface input were within a 2.5% error. The details of the model validation are presented in Appendix B. Notably, the thin layers of shell and addition were taken into account in the interface equation used in the code. Calculations were also performed using a simplified version of this equation in which the thin layer of shell was ignored. It is worth mentioning that the thermal resistances calculated were identical regardless of

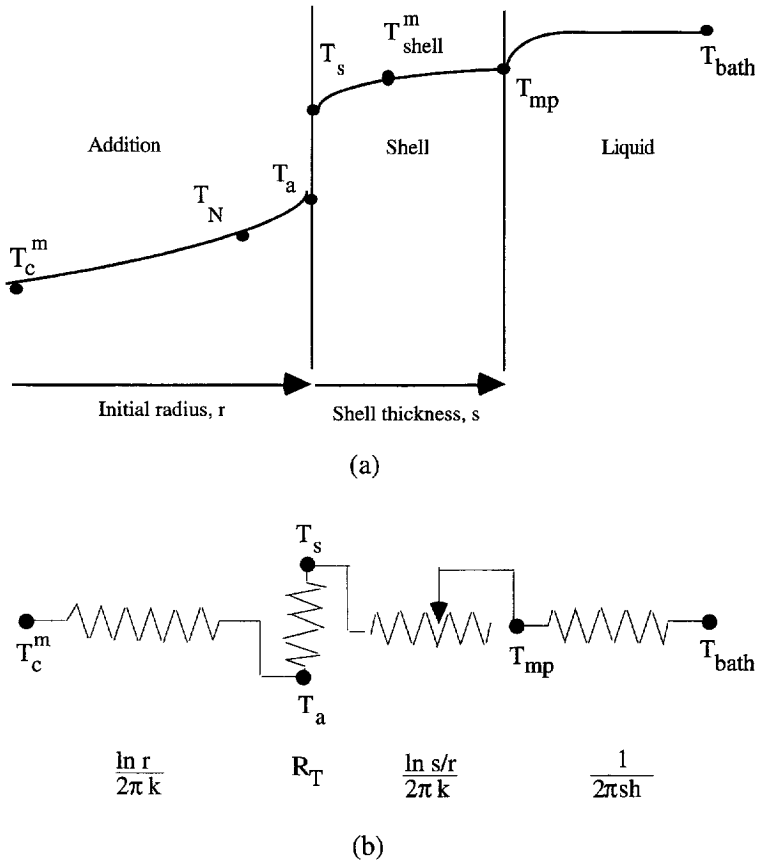

Fig. 5. (a) Schematic illustration and (b) electrical analogy of the thermal resistance at the addition–shell interface per unit length of the cylinder.

Table 2. Thermophysical properties

	Immersed metals				
	Al [16]	Cu [16]	Fe [17]	Mo [16]	Ti [16]
k, W/mK	238.0	397.0	29.8	137.0	21.6
ρ, kg/m^3	2700.0	8960.0	7200.0	10200.0	4500.0
C_p, J/kgK	917.0	386.0	655.0	251.0	528.0
α, m^2/s	96.1×10^{-6}	114.8×10^{-6}	6.3×10^{-6}	53.5×10^{-6}	9.1×10^{-6}
γ, K^{-1}	23.5×10^{-6}	17.0×10^{-6}	13.0×10^{-6}	5.1×10^{-6}	8.9×10^{-6}

	Shell metals		
	Al	Pb	Sn
T_{mp}, K	933.5	600.6	505.1
k, W/mK	215.0	31.8	60.4
α, m^2/s	96.1×10^{-6}	23.0×10^{-6}	44.4×10^{-6}
γ, K^{-1}	23.5×10^{-6}	29.0×10^{-6}	23.5×10^{-6}

Table 3. Input data

Radius, r	0.0127 m
Nodes	30
Grid spacing, dr	4.305×10^{-4} m
Time step, dt	1.0×10^{-4} s

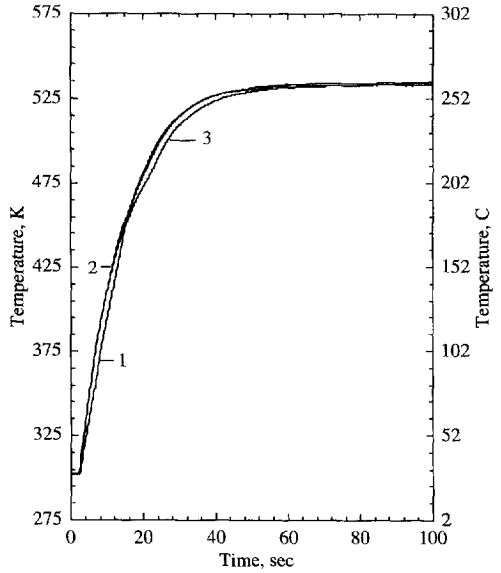

Fig. 6. Measured temperatures for a type-A aluminum specimen immersed 12.4 cm into liquid tin. Curves 1–3 are for 7.1, 8.4 and 9.1 cm bore depths, respectively.

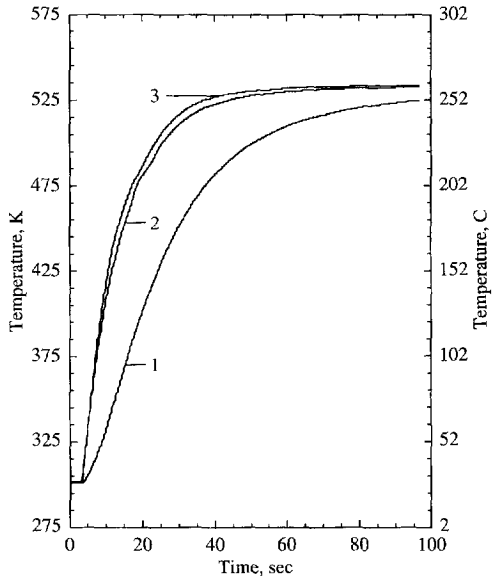

Fig. 7. Measured temperatures for a type-A aluminum specimen immersed 11.4 cm into a liquid tin bath. Curves 1–3 are for 3.4, 8.4 and 13.7 cm bore depths, respectively.

which formula was used. This is important because investigations can therefore be performed using liquids having little, if any, reported thermophysical data, such as industrial slags.

RESULTS

Validation of radial heat flow

Specimen configuration A in Fig. 4 was used to test the 1-dimensional heat flow assumption. Three holes were drilled, 0.8 cm (5/16″) off centre, axially into the specimens. This enabled temperature measurements to be made at an equal radius for different depths. Results for two experiments indicate good agreement with the 1-dimensional, radial assumption. Figure 6 illustrates closely matching temperatures for one specimen with bore depths 7.1, 8.4 and 9.1 cm; curves 1–3, respectively. A decreased slope after approximately 20 s occurs in curve 3, which could be attributed to a poor contact between the cylinder and the thermocouple junction. This particular specimen was immersed 12.4 cm (4 7/8″) into the bath.

Measured temperatures for a specimen with bore depths 3.4, 8.4 and 13.7 cm immersed 11.4 cm (4 1/2″) into the bath are shown in Fig. 7. Since the thermocouple corresponding to curve 1 was actually 0.4 cm above the liquid surface, a lower heat flux was expected compared to that where the thermocouples were at lower depths. Curves 2 and 3 illustrate the higher flux into the cylinder below the liquid surface. Curve 3 shows the quickest temperature changes because the corresponding thermocouple was 5.3 cm below that for curve 2; in fact, only 1.5 cm from the bottom of the specimen. A much steeper slope would be expected for curve 3 if the axial heat flow were dominant. This is not the case; on the contrary, despite the added axial heat flow, it is quite similar to that of curve 2.

The data collected from these experiments indicate that the 1-dimensional assumption is valid.

Experimental data for thermal resistance estimations: centreline and shell temperatures

Specimen configurations B and C were used for the thermal resistance experiments. Typical measured shell and centreline temperatures, represented by curves denoted T^m_{shell} and T^m_c, for these immersion tests are shown in Fig. 8. In this figure, time zero corresponds to time at which the data acquisition system started measuring data. Segment AB, in T^m_{shell}, represents time zero corresponding to the point at which the shell thermocouple enters the liquid bath. The temperature peaks then drops due to immediate shell formation. A minimum temperature is reached along segment BC, at C, as heat is rapidly absorbed by the

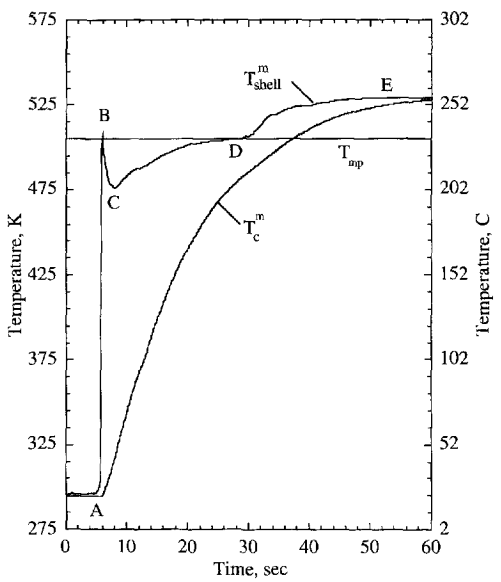

Fig. 8. Typical experimental results for aluminum immersed into tin. Curves T^m_{shell} and T^m_c denote the shell and centreline temperatures, respectively. The melting point of tin is given by T_{mp}.

aluminum cylinder causing the tin surrounding the cylinder to solidify. Initially, the shell grows due to the fact that heat is absorbed into the interior of the cylinder at a much higher rate than the heat which is convected from the metal bath into the cylinder. The relevant energy balance can be written as

$$\rho_s L_s \frac{dS}{dt} = k_s\left(\frac{T_{mp} - T_s}{S}\right) - h_c(T_{bath} - T_{mp}) \quad (4)$$

where the velocity of the solidifying interface dS/dt depends on the difference between the heat conducted away from and convected to the shell–liquid interface, and the thermophysical properties of the shell metal. A balance is maintained by the release of latent heat as the liquid solidifies until a maximum shell thickness is formed. The maximum shell thickness occurs when a zero heat balance at the solid–liquid interface is obtained. Immediately afterwards, the reverse follows and latent heat is required as the shell melts back. Shell formation can be outlined in terms of the velocity of the solidifying interface as follows:

$$\text{Solidification } \frac{dS}{dt} > 0$$

Heat Conducted = Heat Convected + Latent Heat

$$\text{Maximum } \frac{dS}{dt} = 0$$

Heat Conducted = Heat Convected

$$\text{Melt back } \frac{dS}{dt} < 0$$

Heat Conducted = Heat Convected − Latent Heat.

Rapid cooling is followed by heating—segment CD—to the melting point of the shell, signified by the temperature plateau (D). The temperature then increases along segment DE, as the shell–liquid interface recedes past the shell thermocouple, until thermal equilibrium with the bath temperature is attained (E). Temperatures measured during the existence of the shell provided the boundary conditions for computations. Resistances were then calculated based on matching the calculated and measured centreline temperatures.

A typical set of curves for the measured shell T^m_{shell}, and centreline, T^m_c, temperatures, and calculated centreline (curves 1–3) temperatures, T^c_c, are presented in Fig. 9. In this figure, time zero corresponds to the time coordinate of segment AB in Fig. 8. Curves 1–3 illustrate the effect of a thermal resistance at the interface formed by solidifying Sn onto an immersed Al cylinder. These curves represent thermal resistances 5×10^{-5}, 64×10^{-5} and 1000×10^{-5} m^2 K/W, respectively. A low resistance to heat flow across the interface translates into increased heating rates, shown by curve 1. In fact, the calculated centreline temperature approaches a shape similar to the shell temperature curve, and therefore the resistance is effectively approaching zero. Conversely, increased resistance decreases heating rates demonstrated by the small ramping of the centreline temperature in curve 3.

Overall thermal resistances were calculated using a least-squares minimization technique. This is an iterative method which adjusts the thermal resistance values, starting with some

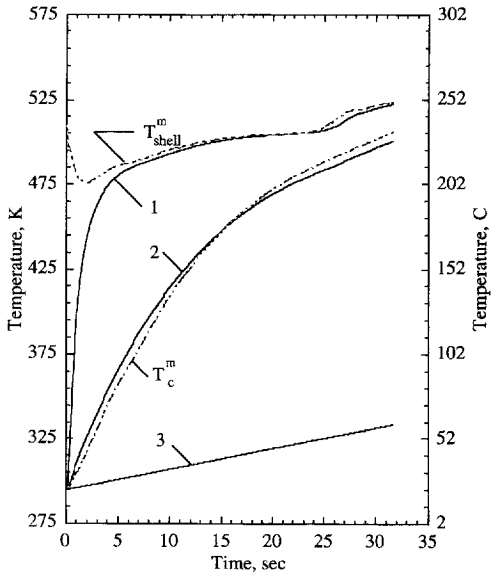

Fig. 9. Curve fitting of the centreline temperature for an aluminum specimen immersed into a liquid tin bath. Curves 1–3 represent calculations with 5, 64 and 1000×10^{-5} m^{2}K/W thermal resistances, respectively.

initial value, by matching specified conditions, and minimizing the squared differences. Centreline temperatures, measured and calculated, were tested in this work to calculate the thermal resistance. Figure 10 illustrates how the code evaluated and corrected the resistance, R_T. An initial value for R_T of 50×10^{-5} m^2 K/W was selected, represented by point A in Fig. 10. Calculations were then made using this initial value, and a comparison between the calculated and measured centreline temperatures completed. Point D corresponds to the total difference between the calculated and measured centreline temperatures. In this particular set of calculations the initial estimate resulted in an overall difference greater than 3300 K. The result was an adjustment to the R_T value as shown by segment AB, which causes the centreline temperatures to be underestimated. This is illustrated by segment DE, where E is the new overall difference of approximately −3000 K. The process continued in this fashion, updating the R_T in relation to the

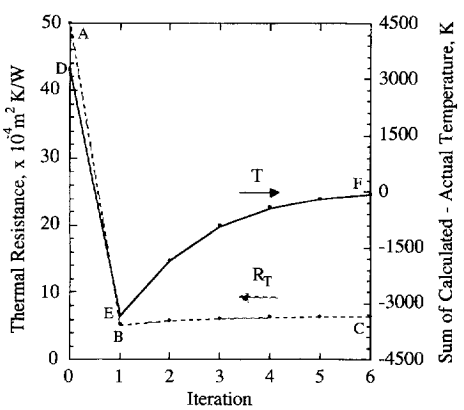

Fig. 10. Iterative calculations of the thermal resistance, R_T, based on a least-squares analysis of the sum of the difference between calculated and measured centreline temperatures, T.

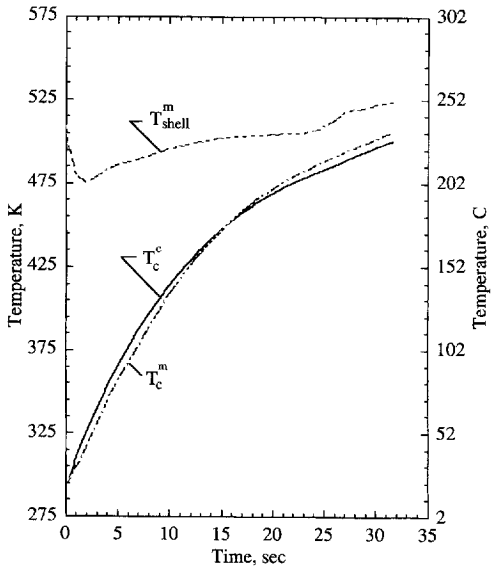

Fig. 11. Comparison of the measured and calculated centreline temperatures, T^m_c and T^c_c, for an aluminum specimen immersed into a liquid tin bath. The thermal resistance was calculated as 64×10^{-5} m^2 K/W for the particular experiment.

calculated overall temperature difference, until the adjustment becomes negligible. Segments BC and EF show how the difference between the calculated and measured centreline temperature approaches zero as R_T becomes optimized. Calculations were terminated when the change in resistance fell below a specified value. The overall thermal resistance for this particular experiment was calculated as 64×10^{-5} m^2 K/W which provided the fit as shown in Fig. 11. Also of interest is the substantial temperature drop at the addition–shell interface where R_T exists; see Fig. 12. In the case of aluminum immersed into liquid tin, the shell–side interface temperature shadows the

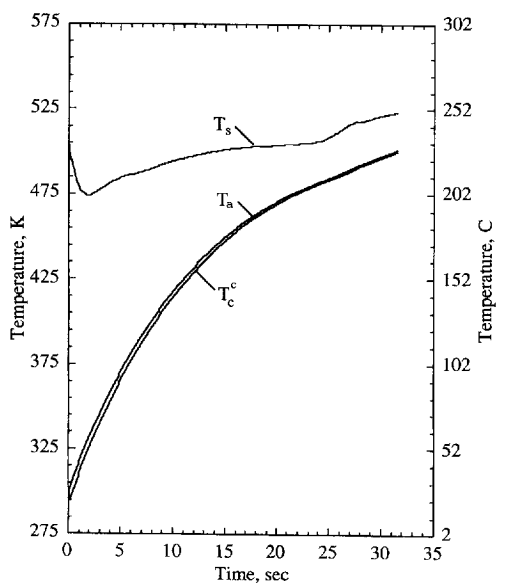

Fig. 12. Calculated temperatures in the aluminum specimen immersed into a liquid tin bath. The temperature drop at the addition–shell interface is illustrated by T_s and T_a.

Table 4. Estimated thermal resistances ($\times 10^5$ m^2 K/W)

	Liquid metal		
Metal immersed	Aluminum	Lead	Tin
Aluminum	40.3	38.6	57.1
Copper	30.8	25.9	40.9
Molybdenum	—	92.2	63.6
Sorel iron	23.9	22.5	27.5
Titanium	49.6	61.3	76.4

shell temperature while the addition–side interface temperature remains close to that of the centreline temperature.

Validation of dynamic temperature measurements

As noted in the discussion of IHCP, the largest component of error in inverse solutions comes from inaccurate temperature data. A method of checking temperature measurements for inaccuracies, therefore, has to be an integral part of any experimental procedure. In the present study, conclusive evidence for the accuracy of the temperature data would be indicated by monitoring whether the highly dynamic temperature measurements reached their plateau at precisely the melting temperature of tin. As can be seen in Fig. 8, the plateau (D) occurred precisely at the melting point of tin. Hence, the accuracy of the temperature measurements are confirmed. This plateau also serves as a thermal analysis of the bath metal, indicating pure tin.

DISCUSSION

Thermal resistance results, averaged over a number of experimental runs, for the different metal combinations investigated are presented in Table 4. These results show that the thermal resistance at the addition–shell interface has a general magnitude of 10^{-5} m^2 K/W. Work performed by other investigators [3–10] in similar systems has also indicated resistances of this magnitude. The most similar experimental configurations (cylindrical) were used by Levy [3], Sun [4] and Mucciardi [7]. Levy [3] estimated conductances for Al immersed into Al alloy 7075 which translate into an overall resistance of 12×10^{-5} m^2 K/W. Mucciardi [7], working with Al in Pb, estimated a thermal resistance of 19×10^{-5} m^2 K/W. Sun [4] determined simple linear relationships with time in terms of conductance for a variety of metal combinations. A corresponding range of 29×10^{-5}–78×10^{-5} m^2 K/W resistances for solid copper in liquid aluminum were calculated from that work. Sun [4] had also speculated that the resistance actually decreases as a function of the pressure exerted at the interface due to the thermal expansion of the cylinder as the shell solidifies and melts. This proposition, however, has never been experimentally tested.

In Fig. 13 the R_T values for different metal combinations have been plotted as a function of the ratio of thermal expansion coefficients for the addition and shell metals. It shows that a higher R_T can be expected when the thermal expansion of the addition is lower than that of the shell metal. Conversely, when thermal expansion of the addition is greater than that of the shell metal, a lower R_T is anticipated. The apparent anomalous

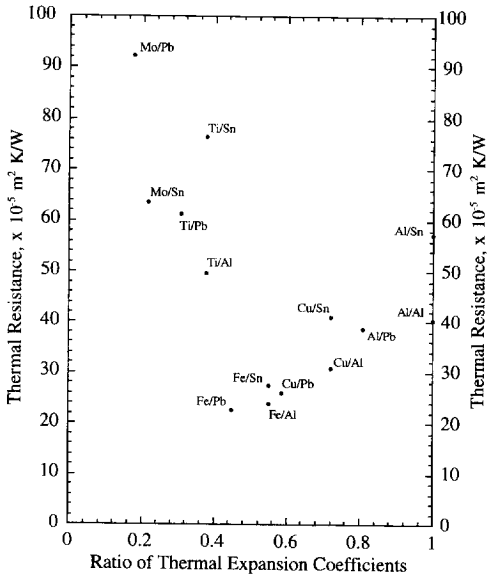

Fig. 13. Thermal expansion effects on interface thermal resistance. The labels indicate the metal combination. For instance, Al/Sn refers to Al immersed into Sn.

R_T estimated for aluminum immersed into liquid tin might be explained by a competing effect from thermal diffusivity, as shown in Table 2. It seems reasonable that the addition–side interface temperature should decrease as the ability of the immersed metal to absorb heat increases. The result would be an increased temperature drop across the interface, which translates into an increased R_T. Higher values of thermal diffusivity accompanied by a high ratio of thermal expansion coefficients tend to lower the R_T value.

CONCLUSIONS

This work represents a low temperature testing of a procedure which involved computational and experimental techniques for estimating interface thermal resistances. Thorough testing of the experimental technique using low temperature liquids is important before moving to the more difficult high melting point metals and slags, since accurate predictions depend on minimizing temperature measurement errors. Immersion of a variety of metal cylinders into several liquid metals was employed to test the technique, and has provided interesting insights into the phenomenon.

Interface thermal resistances in the 10^{-4} and 10^{-5} m^2 K/W range were estimated for the cylindrical specimens immersed into 30° superheated liquid metals. These values fall well within those expected from the literature. Additionally, evidence of thermal expansion and diffusivity effects was presented. It appears from the work that the ratio between added and liquid metal thermal expansion coefficients, as well as the thermal diffusivity, provides an indication of the thermal resistance which can be expected at the interface.

Acknowledgements—The authors thank the University Research Incentive Fund of the Ministry of Colleges and Universities of the province of Ontario for the financial support provided. In addition, the Iron and Steel Society of AIME is acknowledged for its support.

The authors would also like to thank the companies which provided important raw materials for this work: the Noranda Technology Centre, Noranda Inc., for supplying lead bars; Alcan for supplying aluminum bars; and Climax Specialty Metals for the molybdenum cylinders.

REFERENCES

1. C. V. Madhusudana and L. S. Fletcher, Contact heat transfer—the last decade. *AIAA J.* **24**, 519 (1986).
2. T. S. Prasanna Kumar and K. Narayan Prabhu, Heat flux transients at the casting/chill interface during solidification of aluminum base alloys. *Metallurgical Trans. B* **22**, 717 (1991).
3. S. A. Levy, S. Lipson and H. Rosenthal, Influence of a locking chill in solidification time and dendrite arm spacing of cast 7075 aluminum alloy. *AFS Cast Metals Res. J.* **5**, 9 (1969).
4. R. C. Sun, Simulation and study of surface conductance for heat flow in the early stage of casting. *AFS Cast Metals Res. J.* **6**, 105 (1970).
5. M. Prates and H. Biloni, Variables affecting the nature of the chill zone. *Metallurgical Trans. A* **3**, 1501 (1972).
6. S. R. Robertson and E. F. Fascetta, An analytical technique for the determination of the thermal contact resistance between a solidifying metal and mold. *Metallurgical Trans. B* **8**, 619 (1977).
7. F. Mucciardi, Heat flow to cylinders submerged in liquid metal baths. M. Eng. thesis, McGill University, Canada (1977).
8. A. Garcia and M. Prates, Mathematical model for the unidirectional solidification of metals: I. Cooled molds. *Metallurgical Trans. B* **9**, 449 (1978).
9. K. Ho and R. D. Pehlke, Metal–mold interfacial heat transfer. *Metallurgical Trans. B* **16**, 585 (1985).
10. N. A. El-Mahallawy and A. M. Assar, Effect of melt superheat on heat transfer coefficient for aluminum solidifying against copper chill. *J. Mater. Sci.* **26**, 1729 (1991).
11. J. V. Beck, B. Blackwell and C. R. St Clair Jr, *Inverse Heat Conduction: Ill-posed Problems*. John Wiley, New York (1985).
12. E. Hensel, *Inverse Theory and Applications for Engineers*. Prentice-Hall, New York (1991).
13. O. M. Alifanov, *An Introduction to the Theory of Inverse Heat Transfer Problems*. Mashinestroenie Publishing Agency, Moscow (1991).
14. M. N. Ozisik, *Heat Conduction* (2nd Edn), pp. 571–616. John Wiley, New York (1993).
15. F. P. Incropera and D. P. De Witt, *Fundamentals of Heat and Mass Transfer*, p. 245. John Wiley, New York (1990).
16. E. Brandes (ed.), *Smithells Metals Reference Book* (6th Edn). Butterworth, London (1983).
17. C. Sharpe (ed.), *Kempe's Engineers Year-book* (Vol. 1). Benn Business Information Services Ltd, Tonbridge, Kent (1993).
18. P. J. Schneider, *Conduction Heat Transfer*, pp. 245–255. Addison-Wesley, New York (1955).

APPENDIX A

Derivation of the interface temperature formulae

A quasi-steady state heat balance was performed at the interface that occurs when a liquid metal solidifies, and melts back, against a cylindrical metal addition immersed into that liquid. Figure 14 elaborates on the details of the nodal point configuration around the interface. It shows that the last node of the nodal network resides at a distance $dr/2$ from the interface where the two interface temperatures are located. Also, the shell thermocouple junction is positioned a distance Δr from the interface in the shell. The heat balance at the interface can be written

$$q_a = q_i = q_s, \tag{A1}$$

which states that the rate of heat passing the interface, q_i, must be equal to both that entering the interface from the shell, q_s, and that leaving the interface into the addition, q_a. The heat rate equations are as follows. For the addition–side of the interface:

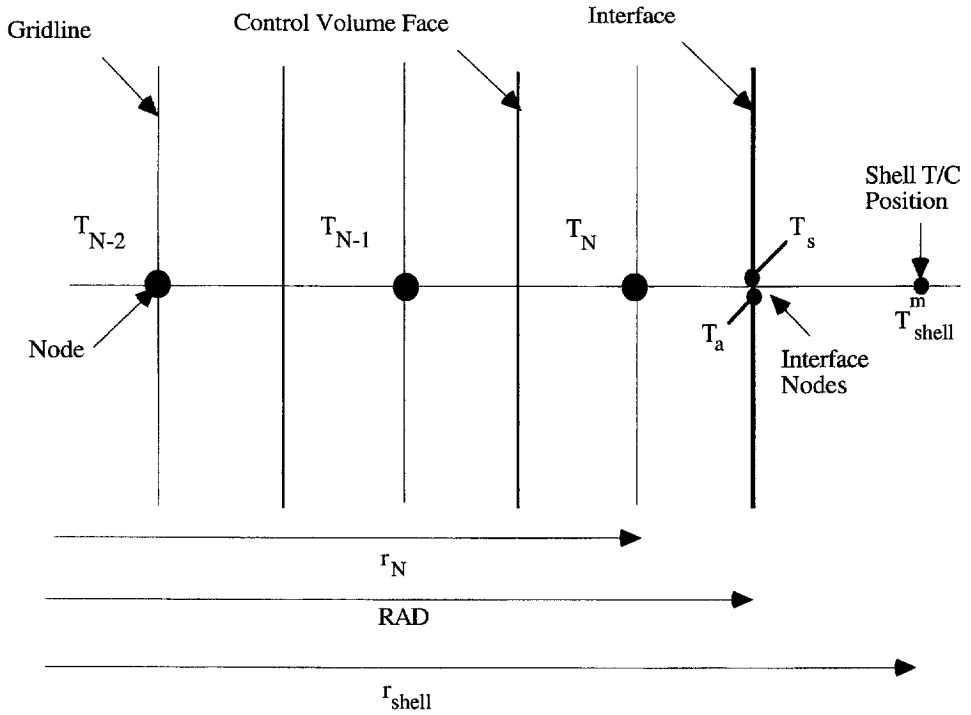

Fig. 14. Details of the nodal network near the interface.

$$q_a = \frac{2\pi k_a (T_N(t) - T_a(t))}{\ln\left(\frac{RAD}{RAD - dr/2}\right)}; \tag{A2}$$

at the interface:

$$q_i = \frac{2\pi RAD\,(T_a(t) - T_s(t))}{R_T}; \tag{A3}$$

and at the shell–side of the interface:

$$q_s = \frac{2\pi k_s (T_s(t) - T^m_{\text{shell}}(t))}{\ln\left(\frac{RAD + \Delta r}{RAD}\right)}. \tag{A4}$$

The addition–side interface temperature, $T_a(t)$, can be derived solving the addition–side of the overall heat balance. That is,

$$\frac{2\pi k_a (T_N(t) - T_a(t))}{\ln\left(\frac{RAD}{RAD - dr/2}\right)} = \frac{2\pi RAD\,(T_a(t) - T_s(t))}{R_T}. \tag{A5}$$

Algebraic manipulation of this balance gives the $T_a(t)$ equation, in terms of $T_N(t)$ and $T_s(t)$, as follows:

$$T_a(t) = \frac{k_a T_N(t) + \dfrac{RAD \ln\left(\frac{RAD}{RAD - dr/2}\right)}{R_T} T_s(t)}{k_a + \dfrac{RAD \ln\left(\frac{RAD}{RAD - dr/2}\right)}{R_T}}. \tag{A6}$$

A similar manipulation is performed with q_i and q_s to give the $T_s(t)$ equation, in terms of $T^m_{\text{shell}}(t)$ and $T_a(t)$, as follows:

$$T_s(t) = \frac{k_s T^m_{\text{shell}}(t) + \dfrac{RAD \ln\left(\frac{RAD + \Delta r}{RAD}\right)}{R_T} T_a(t)}{k_s + \dfrac{RAD \ln\left(\frac{RAD + \Delta r}{RAD}\right)}{R_T}}. \tag{A7}$$

Simplifications to these equations help to solve for the final forms. These simplifications were to set the radial distances as

$$\delta r_N = RAD \ln\left(\frac{RAD}{RAD - dr/2}\right) \tag{A8}$$

$$\delta r_{\text{shell}} = RAD \ln\left(\frac{RAD + \Delta r}{RAD}\right). \tag{A9}$$

Furthermore, thermal conductivity and R_T were incorporated into the thermal coefficients:

$$K_a = k_a + \frac{\delta r_N}{R_T} \tag{A10}$$

$$K_s = k_s + \frac{\delta r_{\text{shell}}}{R_T}. \tag{A11}$$

Making the appropriate substitutions of (A8)–(A11) into (A6) and (A7), the modified equations become:

$$T_a(t) = \frac{k_a T_N(t) + \dfrac{\delta r_N T_s(t)}{R_T}}{K_a} \tag{A12}$$

$$T_s(t) = \frac{k_s T^m_{\text{shell}}(t) + \dfrac{\delta r_{\text{shell}} T_a(t)}{R_T}}{K_s}. \tag{A13}$$

The final form of $T_a(t)$ must use $T^m_{\text{shell}}(t)$, which comes from the experimental data; therefore, (A13) was substituted into (A12) to obtain:

$$T_a(t) = R_T\left(\frac{R_T K_s k_a T_N(t) + \delta r_N k_s T^m_{\text{shell}}(t)}{R_T^2 K_a K_s - \delta r_N\, \delta r_{\text{shell}}}\right) \tag{A14}$$

$$T_s(t) = \frac{k_s R_T T^m_{\text{shell}}(t) + \delta r_{\text{shell}} T_a(t)}{R_T K_s}. \tag{A15}$$

APPENDIX B

Analytical validation of the numerical code

Schneider [18] provided the analytical solution for radial heat flow in an infinite cylinder with variable temperature which can be written in the dimensionless form as:

$$\theta^* = \sum_{n=1}^{\infty} C_n \exp(-\zeta_n^2 F_o) J_0(\zeta_n r^*) \tag{B1}$$

where

$$C_n = \frac{2}{\zeta_n}\frac{J_1(\zeta_n)}{J_0^2(\zeta_n) + J_1^2(\zeta_n)}.$$

The one-term approximation is appropriate for this test because the solution of Bessel's equation of the second kind is infinite at $r = 0$; therefore, the form is written as

$$\theta^* = C_1 \exp(-\zeta_1^2 F_o) J_0(\zeta_1 r^*). \tag{B2}$$

The numerical code was tested using a simplified interface temperature equation

$$T_a(t) = \frac{\left(\frac{1}{R_T}\right) T^m_{\text{shell}}(t) + \frac{k_a}{\mathrm{d}r/2} T_N(t)}{\left(\frac{1}{R_T}\right) + \frac{k_a}{\mathrm{d}r/2}}, \tag{B3}$$

derived from a simplified heat balance at the interface which used only the thermophysical properties of the cylindrical addition. This allowed the problem to be approached as a convective heat transfer coefficient problem with the heat flux given as

$$q'' = h_c(T_a(t) - T^m_{\text{shell}}(t)) \tag{B4}$$

where h_c is effectively $1/R_T$.

Numerical and analytical results for three convective conditions, denoted by the Biot numbers, are compared in Fig. 15. The numerical results, depicted by the points, accurately follow the analytical solutions for Biot numbers 0.01, 0.1 and 1.0. A small deviation occurs only for 1.0 at the start because the analytical solution calculates the initial value for the centreline temperature, θ_0^*, as 1.2, whereas the code has the initial temperature set so that θ_0^* equals 1.0. It should be noted that the Biot number of unity represents a significantly large heat transfer coefficient. Consider the aluminum cylinder of radius 0.0127 m. Given a thermal conductivity of 238 W/mK, the heat transfer coefficient would be significantly large at 18740 W/m^{2}K.

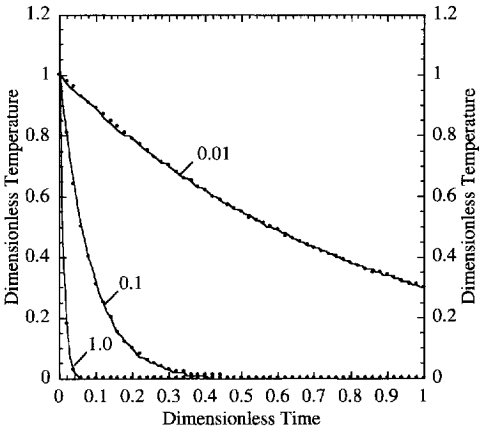

Fig. 15. Transient centreline temperature in a cylinder for different convective conditions as indicated by the Biot numbers assigned to each curve. The solid line shows the approximate analytical solution, while the points depict results from the numerical model.

An integral heat balance was also conducted in order to check the performance and accuracy of the code. A balance at each iteration and also overall was performed by calculating the heat content and comparing it with the heat input at the interface. The algorithm can be represented in the following mathematical form.

Heat content (HC) of the cylinder

$$\text{HC} = \sum_{t=0}^{t_{\text{total}}} \sum_{n=1}^{\text{Nodes}} \rho C_p V_n (T_n(t) - T_n(t-1)) \tag{B5}$$

where

$$V_n = 2\pi(n-1)\,\mathrm{d}r^2$$

$$V_1 = \tfrac{1}{4}\pi\,\mathrm{d}r^2$$

are the control volumes for each nth node for unit length.

Interface heat input (IHI) to the cylinder

$$\text{IHI} = \sum_{t=0}^{t_{\text{total}}} \frac{2\pi RAD\,(T_a(t) - T_s(t))\,\mathrm{d}t}{R_T}. \tag{B6}$$

Percentage error

$$\frac{|\text{IHI} - \text{HC}|_{100}}{\text{HC}}. \tag{B7}$$

Results from the balance gave a consistent 2.5% error, both overall and at each iteration.